Transportation Geotechnics 39 (2023) 100946

Contents lists available at ScienceDirect

Transportation Geotechnics

journal homepage: www.elsevier.com/locate/trgeo

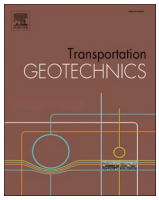

Model development to Predict Dynamic Interactions of Roller and Geomaterial using Simulated Roller Compaction

Amir Tophel [a], Jeffrey P. Walker [b], Troyee Tanu Dutta [a], Didier Bodin [c], Jayantha Kodikara [a,*]

[a] ARC Industrial Transformation Research Hub (ITRH) – SPARC Hub, Dept. of Civil Engineering, Monash University, Clayton Campus, VIC 3800, Australia
[b] Dept. of Civil Engineering, Monash University, Clayton Campus, VIC 3800, Australia
[c] Australian Road Research Board (ARRB), Port Melbourne, VIC 3207, Australia

ARTICLE INFO

Keywords:
Contact Stress
Wheel Tracker
Plastic Deformation
Roller Compaction
Modulus
Density

ABSTRACT

Crushed rock or unbound granular materials constitute the top layer of geomaterial compacted in a pavement. These materials are required to be compacted using compactors or rollers at a designated target density or modulus for satisfactory performance. Studying the interaction between compactors and geomaterial is important for optimising these geomaterial layers' construction. As field compaction is time-consuming and cumbersome, the study of material behaviour at a smaller scale is necessary. This study utilises a novel setup simulating the field compaction better to study the material's behaviour and dynamic interaction between the material and the compactor during compaction. A constitutive model was developed utilizing the geometric relationship between the contact width to plastic deformation during compaction, which can be easily measured. Using Hertzian theory, the estimation of contact width allows the estimation of contact stress. The developed model shows that it can model the experimental observation with very high accuracy ($R^2 > 0.98$). The model is then used to predict other geomaterial properties during compaction, showing their dependence on the material state.

Introduction

Construction of roads, dam embankments and bridges are the major activities in the civil engineering domain. These activities are very important to cope with the ever-increasing population. All of these construction activities require an assessment of the suitability of the ground condition of a construction location, including the geomaterial layers on which a structure is built. For instance, if the geomaterial is weakly compacted, a structure built over it will not operate well, and in the case of a road, the service life of the road is lowered, leading to premature failure. The construction of geomaterial layers to specified dry density (ρ_d) or void ratio (e) and other geomaterial properties (e.g., stiffness (K), modulus (E)) are typically required for the quality assurance (QA) of engineered compaction.

On top of that, it is also crucial to minimise material variability within geomaterial layers to prevent structural failures resulting from excessive differential deformations. The compaction of geomaterial to a specified property is commonly undertaken using rollers/compactors. Geomaterial compaction is therefore the process of increasing ρ_d and thus reducing e by removing air voids by applying loads. When geomaterials are compacted, the geometry of the particles' arrangement is altered, resulting in a better packing arrangement and an increase in ρ_d. The compaction process is very complex to explain scientifically in detail. Hence, there are many issues with the current approaches.

First, capturing the cyclic loading and unloading process during compaction is an ongoing challenge because the material is unsaturated constituting the three-phase media. Numerous researchers have attempted to model the behaviour of unsaturated materials under complicated cyclic loads at the laboratory scale using complex analytical and finite element models [1–6]. These models capture some of the complicated behaviour well, but the determination of model parameters requires complex time-consuming experiments, especially for unsaturated geomaterials. A simplified constitutive model was proposed by Sawicki et al. [7], which was recently modified by the authors of this paper [8], who showed that for practical purposes a simplified model could be used to capture the essential physics of the compaction process. This model requires fewer material parameters and is advantageous, especially when aiming at future real-time applications. Unfortunately, similar to other constitutive models, the model needs applied parameters such as stress as an input, which is variable during compaction.

* Corresponding author.
E-mail addresses: amir.tophel@monash.edu (A. Tophel), jeff.walker@monash.edu (J.P. Walker), troyee.dutta@monash.edu (T.T. Dutta), didier.bodin@arrb.com.au (D. Bodin), jayantha.kodikara@monash.edu (J. Kodikara).

https://doi.org/10.1016/j.trgeo.2023.100946
Received 25 October 2022; Received in revised form 22 January 2023; Accepted 24 January 2023
Available online 28 January 2023
2214-3912/© 2023 Elsevier Ltd. All rights reserved.

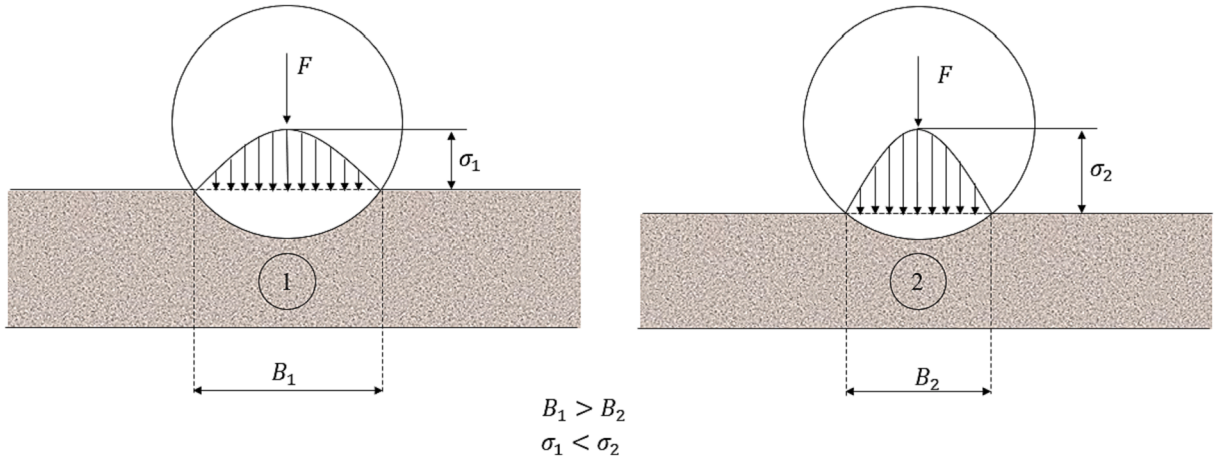

Fig. 1. Interaction between cylindrical roller compactor and material with different states: (a) loose state (state 1); (b) dense state (state 2).

The compaction process modelling using rollers is challenging due to the change in the geomaterial properties (stiffness, ρ_d, modulus) and geomaterial-compactor interactions (contact width, contact stress) during compaction [9,10]. For example, Ghorbani et al. [11] used the advanced mortar-type contact algorithm to model a cylinder and geomaterial contact evolution and found that the contact width reduces with an increase in ρ_d. Because of this reduction in roller/material contact area during compaction, the contact stress increases as compaction progresses even though the load applied due to the compactor remains pretty much the same. The stresses applied by a cylindrical compactor can be evaluated approximately using Hertz's theory [12], which has been verified using field measurements [13,14]. However, calculating the stresses using the Hertzian approach requires knowledge of either Young's modulus or the contact width of the compacted material, both of which change during compaction. As these two parameters are difficult to measure or estimate during the compaction process, most detailed numerical modelling approaches assume the parameters are constant during the simulation, which limits the models' capability. For example, both [15] and [11] considered the modulus of the geomaterial to be constant during compaction. However, it has been demonstrated that the modulus depends on the ρ_d and increases as the ρ_d increases during compaction [16]. This study exploits a geometrical relationship between the plastic deformation during compaction and the associated contact width, and, thereby, presents a nonlinear relationship between the contact stress and the plastic deformation during compaction. The plastic deformation was selected as the independent variable as this can be measured relatively easily compared to contact width. For instance, it can be measured by using either contact or non-contact displacement sensors in the laboratory or in the field using scanning measurement systems and or advanced instrumentation [17–19]. This hypothesis allows the estimation of stresses needed for a constitutive (i.e., stress–strain) relationship using only the load applied, which is easier to determine during compaction.

The third issue related to compaction is the variation of initial density (ρ_{d0}) or initial void ratio (e_0). Because different techniques are used to place and spread the geomaterial, the initial placement ρ_{d0} or e_0 can vary, even for the same material with a particular moisture content. Due to the use of different machinery, the initially applied energy can be different, leading to different e_0. Hence, the void ratio evolution (change in void ratio during compaction) can be different even for the same applied load during roller compaction. This study also explores the effect of e_0 on void ratio evolution during simulated roller compaction.

Experimental evidence was used in this paper to develop a model to study stiffness, modulus, contact area, contact stresses and their evolution during compaction. The typical variation of these properties is reported, and their relationships with factors such as void ratio, number of cycles, and initial state are presented. Such information can be used in constitutive modelling instead of considering them to be constant during compaction.

On the basis of experiments undertaken on unbound granular materials (UGM), the model was validated and the issues noted above are addressed. The compaction was performed using a novel steel foot compactor simulating drum compaction in the field. The effects of the initial density, moisture and plasticity of fines on the compaction characteristics and model parameters were also studied.

Model development

Hertzian contact theory and geometrical relationship between contact width and plastic deformation

When a stationary cylindrical drum is in contact with geomaterial in loose condition, the contact width/area is higher than when the same roller is applied to a denser material as the indentation of the roller at the material's surface decreases with the increasing density [12]. Fig. 1 (a) and 1(b) illustrate the difference in the interaction between the roller and the material when the material is in the loose and dense states, respectively.

When the material is in a loose state, the contact width (B) is higher, and hence, under the same vertical load F, the stress is lower. The contact width keeps reducing with an increase in the number of cycles (or the number of rollers passes), and the contact stress increases during compaction even when the load (F) is constant. Constitutive relationships to model the compaction process require knowledge of the stresses. However, variable contact width and stresses during compaction make the modelling of the roller compaction process challenging.

For a cylinder contacting the elastic half media, the contact stress can be evaluated using Hertzian contact theory [12] as

$$\frac{1}{E^*} = \frac{1-\nu_1^2}{E_1} + \frac{1-\nu_2^2}{E_2} \tag{1}$$

$$\sigma^2 = \frac{E^* F}{\pi L R} \tag{2}$$

where, E^* is the equivalent modulus of the system, (E_1, ν_1) and (E_2, ν_2) are the Young's modulus and the Poisson's ratio of the geomaterial and the cylindrical compactor respectively. F is the load applied by the cylindrical compactor, whereas L is the length of the compactor, R is the radius of the compactor, and σ is the maximum contact stress. For this study, ν_1, E_2 and ν_2 were considered as a constant during compaction with the values of 0.35, 200 GPa and 0.2 respectively.

Using Equations (1) and (2), the contact stress can be estimated but

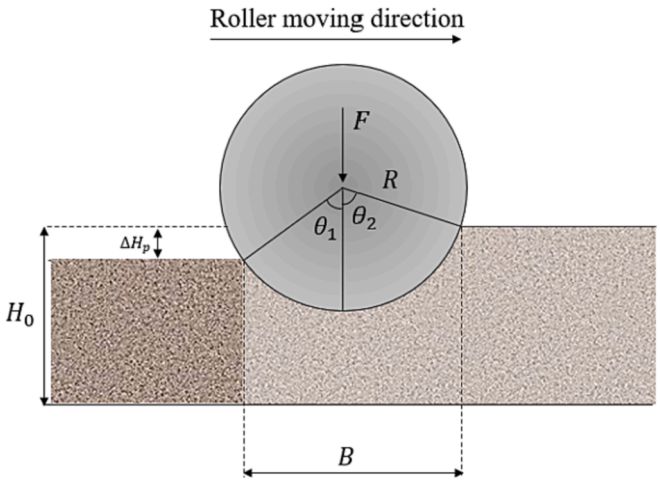

Fig. 2. Interaction between cylindrical compactor and geomaterial during compaction.

the knowledge of the modulus of the geomaterial is needed. Similar to the stresses and contact width, the modulus of the geomaterial also changes during compaction. Accordingly, the contact width (B) can be determined according to Hertzian theory [12] as

$$B = \sqrt{\left(\frac{16RF}{\pi E^* L}\right)} \tag{3}$$

From Equations (2) and (3), the peak contact stress can be written in terms of the contact width and the load applied such that

$$\sigma = \frac{4F}{\pi LB} \tag{4}$$

Fig. 1 depicts an idealised form of interaction between cylinder and geomaterial when the cylinder is stationary and the load is vertical. But in reality, the cylinder moves in a horizontal direction while applying the load vertically (Fig. 2). This study utilises the geometrical relationship between plastic deformation or compaction which is the difference between the front and back of the compactor (ΔH_p) and contact width (B) as shown.

From the above figure, the contact width can be written in terms of R and the internal angles (θ_1, θ_2) that it makes with the contact area with such that

$$B = R\big(sin(\theta_2) + sin(\theta_1)\big) \tag{5}$$

and the plastic deformation (ΔH_p) as

$$\Delta H_p = R\big(cos(\theta_1) - cos(\theta_2)\big) \tag{6}$$

Comparing the two variables using the trigonometric identities, contact width takes the form

$$B = 2Rsin\left(\frac{\theta_1 + \theta_2}{2}\right) cos\left(\frac{\theta_1 - \theta_2}{2}\right) \tag{7}$$

and the equation for plastic deformation (Equation (6)) is reduced to

$$\Delta H_p = 2Rsin\left(\frac{\theta_1 + \theta_2}{2}\right) sin\left(\frac{\theta_2 - \theta_1}{2}\right) \tag{8}$$

Equations (7) and (8) show that B and ΔH_p are related during a compaction cycle, i.e. $B \propto \Delta H_p$. Based on the experimental evidence of this study (shown later), it can be assumed that these two variables are related using a power function such that

$$B = \alpha \Delta H_p^{\beta} \tag{9}$$

where α and β are two additional constitutive parameters that depend on the geometric properties of the compactor.

Using Hertzian contact theory, the maximum stress due to a cylinder can be recast based on Equations (4) and (9) such that

$$\sigma = \frac{4F}{\pi L \alpha \Delta H_p^{\beta}} \tag{10}$$

It should be noted that when ΔH_p becomes zero the situation corresponds to the point loading problem. Because of the point load, the contact stress becomes infinite and a similar observation can be made when using the Boussinesq's equation to estimate the stresses due to point load. In the field, when compaction process becomes stationary at the end of the compaction, ΔH_p tends to go to zero at and in turn the contact stress becomes very high.

Modification of stress-based model to a load-based model

Sawicki et al. [7] developed a constitutive model in 1D compression, which was later progressed by Tophel et al. [8]. In this work, the cumulative plastic strain (ϵ_p) was considered to evolve logarithmically with the cycle number (N) subjected to a vertical stress (σ_z) such that

$$\epsilon_p = C_1 ln\left(1 + N\left(\frac{\sigma_z}{\sigma_{ref}}\right)^m\right), \tag{11}$$

where C_1 and m are model parameters and $\sigma_{ref} = 1$ kPa.

The above equation can then be differentiated to provide incremental plastic strain, i.e. ($\frac{d\epsilon_p}{dN} or \Delta\epsilon_p$) yielding

$$\Delta\epsilon_p = C_1\left(\frac{\sigma_z}{\sigma_{ref}}\right)^m exp(-\frac{\epsilon_p}{C_1}) \tag{12}$$

Equation (12) is represented in terms of incremental plastic deformation (ΔH_p) and initial height (H_0) and cumulative plastic deformation (H_p) such that

$$\Delta H_p = H_0 C_1\left(\frac{\sigma_z}{\sigma_{ref}}\right)^m exp(-\frac{H_p}{H_0 C_1}) \tag{13}$$

As stated earlier, the load is commonly known during compaction, but not the stress. Therefore, Equation (13) is modified by adding the two constitutive parameters introduced in Equation (9) such that

$$\Delta H_p = H_0 C_1\left(\frac{4F}{\pi L \alpha \Delta H_p^{\beta}}\right)^m exp(-\frac{H_p}{H_0 C_1}) \tag{14}$$

The stress term is then replaced by the maximum stress applied by the cylindrical compactor during compaction. The maximum stress is taken as the shear failure responsible for the plastic deformation is due to the maximum stress. By rearranging,

$$\left(\Delta H_p\right)^{1+\beta m} = H_0 C_1\left(\frac{4F}{\pi L\alpha}\right)^m exp(-\frac{H_p}{H_0 C_1}) \tag{15}$$

Equation (15) can be integrated for either a constant or variable load condition.

If the applied load is not constant, integration of Equation (15) yields

$$H_p = H_0 C_1 (1 + \beta m) ln\left(1 + \frac{1}{1 + \beta m}\left(\frac{4}{\pi L\alpha}\right)^m \int_0^N F^m dN\right). \tag{16}$$

For a constant load, Equation (16) can be integrated to determine the cumulated material surface deformation

$$H_p = H_0 C_1 (1 + \beta m) ln\left(1 + \frac{1}{1 + \beta m}\left(\frac{4F}{\pi L\alpha}\right)^m N\right). \tag{17}$$

Assuming the material properties constant with depth in the compacted layer, the void ratio e_N at cycle, N can be calculated form the initial void ratio and height e_0 and H_0 respectively using the following equation approximately:

Table 1
Evolution of all the parameters (with N and e_N) during compaction.

Parameters		General Equation
Contact width (B)	N	$B = \alpha(H_0C_1)^{\frac{\beta}{1+\beta m}}\left(1+\frac{1}{1+\beta m}\left(\frac{4}{\pi L\alpha}\right)^m\int_0^N F^m dN\right)^{-\beta}$
	e_N	$B = \alpha(H_0C_1)^{\frac{\beta}{1+\beta m}}exp\left(-\frac{\beta}{C_1(1+\beta m)}\times\frac{(e_0-e_N)}{1+e_0}\right)$
Contact Stress (σ)	N	$\sigma = (H_0C_1)^{\frac{-\beta}{1+\beta m}}\left(1+\frac{1}{1+\beta m}\left(\frac{4}{\pi L\alpha}\right)^m\int_0^N F^m dN\right)^{\beta}$
	e_N	$\sigma = (H_0C_1)^{\frac{-\beta}{1+\beta m}}exp\left(\frac{\beta}{C_1(1+\beta m)}\times\frac{(e_0-e_N)}{1+e_0}\right)$
Modulus (E_1)	N	$E_1 = \frac{(H_0C_1)^{\frac{-2\beta}{1+\beta m}}\left(1+\frac{1}{1+\beta m}\left(\frac{4}{\pi L\alpha}\right)^m\int_0^N F^m dN\right)^{2\beta}\times\left(\frac{\pi LR}{F}\right)E_2(1-\nu_1^2)}{E_2-(H_0C_1)^{\frac{-2\beta}{1+\beta m}}\left(1+\frac{1}{1+\beta m}\left(\frac{4}{\pi L\alpha}\right)^m\int_0^N F^m dN\right)^{2\beta}\times\left(\frac{\pi LR}{F}\right)E_2(1-\nu_2^2)}$
	e_N	$E_1 = \frac{(H_0C_1)^{\frac{-2\beta}{1+\beta m}}exp\left(\frac{2\beta}{C_1(1+\beta m)}\times\frac{(e_0-e_N)}{1+e_0}\right)\times\left(\frac{\pi LR}{F}\right)E_2(1-\nu_1^2)}{E_2-(H_0C_1)^{\frac{-2\beta}{1+\beta m}}exp\left(\frac{2\beta}{C_1(1+\beta m)}\times\frac{(e_0-e_N)}{1+e_0}\right)\times\left(\frac{\pi LR}{F}\right)E_2(1-\nu_2^2)}$
Stiffness (K)	N	$K = (H_0C_1)^{\frac{-1}{1+\beta m}}\left(1+\frac{1}{1+\beta m}\left(\frac{4}{\pi L\alpha}\right)^m\int_0^N F^m dN\right)$
	e_N	$K = (H_0C_1)^{\frac{-1}{1+\beta m}}exp\left(\frac{\beta}{C_1(1+\beta m)}\times\frac{(e_0-e_N)}{1+e_0}\right)$

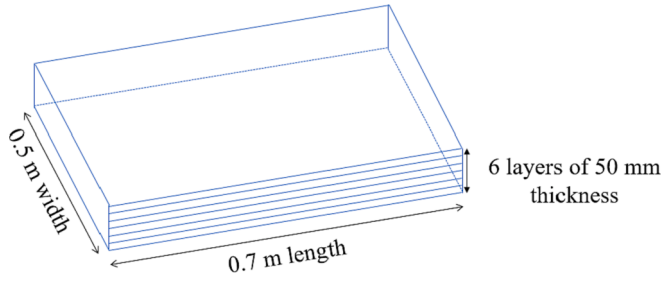

Fig. 3. Dimensions of the compaction mould.

$$\frac{e_0 - e_N}{1+e_0} = \frac{H_p}{H_0} \tag{18}$$

Recalling the inverse relation between void ratio (e) and dry density (ρ_d) can be calculated as

$$\rho_d = \frac{G_s\gamma_w}{1+e} \tag{19}$$

where G_s is the specific gravity and γ_w is the unit weight of water.

The plastic stiffness (K) expresses the relationship between the vertical force (F) and the plastic deformation increment (ΔH_p) and is calculated as follows:

$$K = \frac{F}{\Delta H_p} \tag{20}$$

Similar to the plastic stiffness (K), modulus of the geomaterial represented by E_1, represents the plastic modulus of the geomaterial. Equation (16) can be used to derive all the material properties during compaction and is presented in Table 1.

Materials and Testing method

The experimental data comes from the laboratory compaction of slabs where multiple thin layers are compacted to gradually construct a 300 mm high full depth specimen [20] using the extra-large compactor

Fig. 4. Photo of the segmented roller and specimen during compaction.

and wheel tracker develop by ARRB for Austroads [21]. The materials used in this study were unbound granular materials (UGM) as they constitute the base layer of a flexible pavement and carries most of the load coming from the traffic.

Each sample was compacted in a mould of dimensions (length = 700 mm, width = 500 mm, and height = 300 mm) in six layers (Fig. 3). Each sample (300 mm thick) is compacted in 50 mm layers of 6 layers aiming at producing a uniform specimen with minimum density gradient with depth. In the field, density gradient will be observed with the spread of the compaction load with depth. The compaction in sublayers was developed to allow reducing density gradient even when compacting material below optimum compaction moisture in order to avoid generation of high compaction effort and prevent potential particle breakage during the compaction process when testing weak or marginal fit-for-purpose materials.The material was first homogenised using a rotary splitter and dried at a low temperature (80 °C). Before compaction,

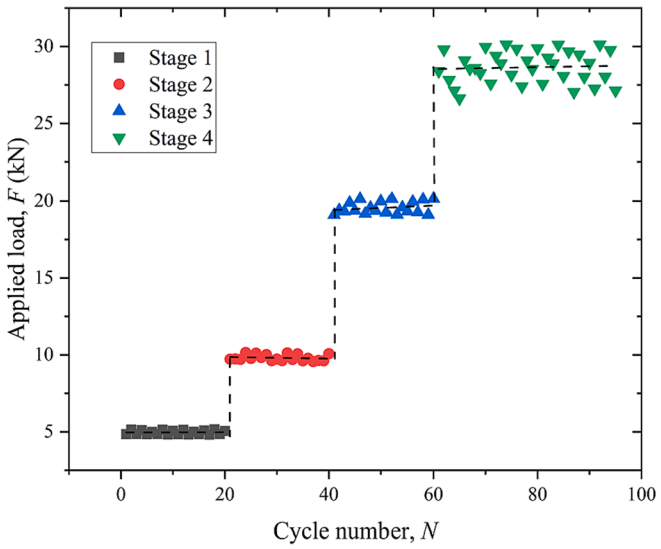

Fig. 5. Loading cycle details for one of the samples.

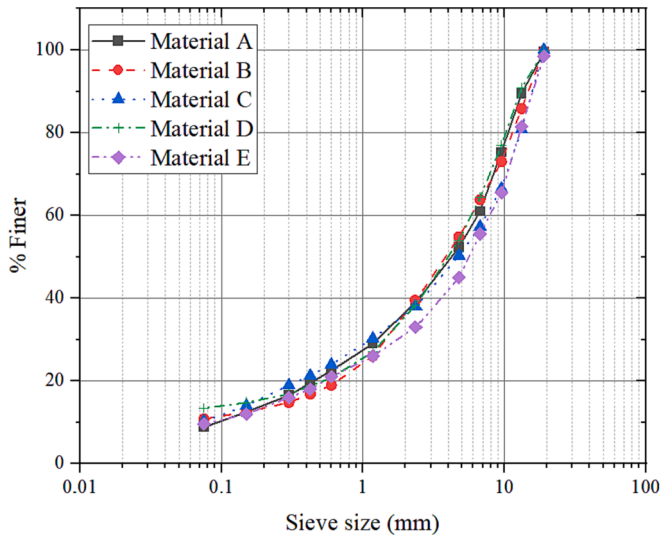

Fig. 6. Grain size distribution (GSD) of all the materials used in this study.

water was added to the dry aggregates to achieve the desired moisture content. Mixing with the appropriate mass of water was performed using an 80-litre concrete mixer. The material was then stored and sealed before compaction.

Based on the targeted density (void ratio) and moisture content, the wet mass required was calculated and the material was spread in the mould. Special care was taken to avoid segregation while spreading. The material was first spread and compacted using a hand-held tamping device to ensure even distribution. The material was then pre-compacted with a load of about 1 kN. The compaction effort or load applied on the steel compaction foot (Fig. 4) was loaded at 5 kN and gradually increased with the measured height for density estimation at the centre of the specimen recorded. by a Linear Variable Differential Transformer (LVDT) displacement sensor. The LVDT is attached between the machine frame and the bottom of the mould. The compaction effort is applied on the specimen mould from underneath pushing the specimen and the material to be compacted towards the compaction foot. Change in displacement results from the thickness reduction of the material in the mould. This interpretation assumes that the deflection of the machine frame and compaction foot is negligible compared to the height variation when compacting the granular material due to significant modulus difference between the steel and the soil. During the compaction of the layer i it is assumed that no further compaction is experienced in the underlying layer i-1 and below, which are already compacted at the target density. The change of relative position of the bottom of the mould / compaction foot radius is interpreted as the change in height of layer i. The single measurement of the height in the middle of the slab was used as a measurement of the density. As during the development of the test method the uniformity of the density achieved in the compacted resulting from the compaction procedure (AGPT/T054) was assessed and demonstrated (except edge effects inherent to compaction of granular materials) as described in ([21]). An example of one loading scenario is shown in Fig. 5. The loading was started at 5 kN (stage 1) until a maximum of 20 cycles and increased to 10 kN (stage 2) for a maximum of 20 cycles if the desired height was not achieved. The loading is further increased to 20 kN (stage 3) and then 30 kN (stage 4) for a maximum of 20 cycles each until the compaction is achieved. Core samples at the end were obtained to verify the density calculated using the height measurement.

Testing Program

The test matrix included 14 samples comprising five different materials and was given different ARRB sample register numbers 2510, 2511, 2512, 2513 and 3850, referred to here simply as materials A, B, C, D, and E, respectively. The details of the materials are given in Table 2 with the grain size distributions shown in Fig. 6.

Materials A and B were sourced from a quarry in Lysterfield, Victoria, Australia and a quarry in Tynong, Victoria, Australia, respectively. Materials C, D, and E were prepared in the lab to study the effect of plasticity. Material C had 6% Claypro (a clay additive) added to material A while material D had 30% Class 4 subbase material (VicRoads classification [22]) added. Material E was planned to be prepared similar to material C, but because of the incorporation of scalping materials to improve the grading, the material became more plastic due to the

Table 2
Results of the basic characterisation tests on each material.

Material	Granite standard plasticity	Hornfels standard plasticity	Granite increased plasticity	Hornfels increased plasticity	Granite increased plasticity+	Test Standard
Material Number	**2510 (A)**	**2511 (B)**	**2512 (C)**	**2513 (D)**	**3850 (E)**	
%fines (less than 0.075 mm)	8.8	10.8	10.3	13.4	9.6	[23]
%sand (4.75 mm −0.075 mm)	43.5	44	40	40.6	35.4	[23]
%gravel (>4.75 mm)	47.7	45.2	49.7	46	55	[23]
Plastic Limit (PL) (%)	26	23	23	28	28	[24]
Liquid Limit (LL) (%)	19	19	14	20	14	[25]
Plasticity Index (PI) (%)	7	4	9	9	14	[26]
Specific Gravity (G_s)	2.66	2.74	2.79	2.74	2.66	[27]
Optimum Moisture Content (OMC), modified Proctor (%)	6.6	5.6	5.5	6.6	5.9	[28]
Maximum Dry Density (MDD), modified Proctor (kg/m^3)	2200	2300	2290	2230	2270	[28]

Table 3
Test matrix used for this study.

Sample ID	Mat. No.	MC (%)
1	A	3.61
2	A	4.32
3	A	4.93
4	A	4.13
5	B	4.02
6	B	4.05
7	B	4.9
8	C	4.07
9	C	4.82
10	C	5.11
11	D	3.94
12	D	5.67
13	E	4.13
14	E	4.9

inclusion of plastic fines.

Different samples of each material were prepared and tested to study the effect of moisture content. Table 3 shows the test matrix of all the samples with the moisture content (MC) used for preparation.

As previously stated, each sample was compacted in six layers, with the manual tamping during sample preparation creating different e_0 for each layer before the actual compaction began. However, these layers were compacted to approximately the same final void ratio (e_{final}). Fig. 7 shows that because of the different e_0, each sample experienced a different number of cycles (N) to reach e_{final}. The initial void ratio and the final/target void ratio matrix for all the samples is shown in Table 4.

Results and discussions:

Prediction ability of the developed model

The prediction model skill was assessed using two metrics, coefficient of correlation (R^2) and mean absolute error (MAE) defined as.

$$\mathrm{MAE} = \frac{1}{len(Y)}\sum_{i=1}^{len(Y)}\left|Y - Y_{pred}\right| \tag{21}$$

$$R^2 = 1 - \frac{\sum_{i=1}^{len(Y)}\left(Y - Y_{pred}\right)^2}{\sum_{i=1}^{len(Y)}\left(Y - \overline{Y}\right)^2} \tag{22}$$

where Y is the experimental observation, Y_{pred} is the predicted output from the model, $\overline{Y}$ is the mean value of all the values of Y, and $len(Y)$

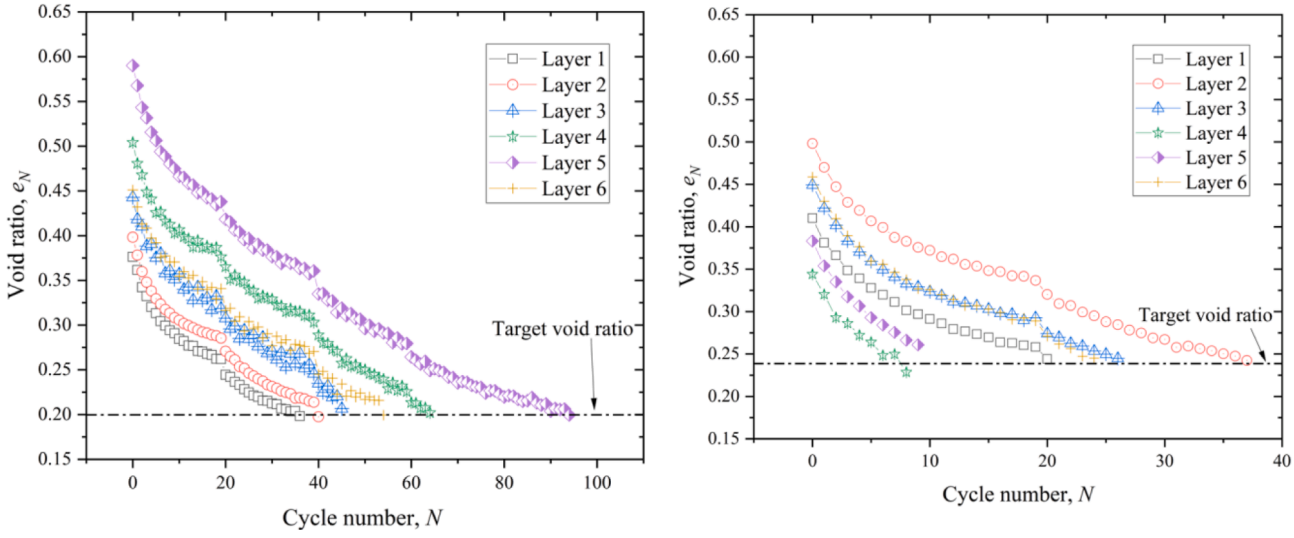

Fig. 7. Void ratio evolution during compaction for each layer for: (a) sample 4, (b) sample 13.

Table 4
The e_0 matrix and e_{final} for all the samples tested.

Sample ID	Initial Void ratio (e_0)						Final void ratio (e_{final})
	Layer 1	Layer 2	Layer 3	Layer 4	Layer 5	Layer 6	
1	0.314	0.516	0.462	0.436	0.490	0.461	0.227 ± 0.007
2	0.394	0.457	0.446	0.471	0.471	0.474	0.227 ± 0.006
3	0.389	0.504	0.418	0.484	0.460	0.505	0.228 ± 0.005
4	0.376	0.398	0.443	0.504	0.590	0.451	0.201 ± 0.003
5	0.399	0.464	0.426	0.439	0.444	0.481	0.227 ± 0.003
6	0.416	0.440	0.434	0.498	0.417	0.605	0.226 ± 0.005
7	0.335	0.434	0.422	0.415	0.457	0.373	0.223 ± 0.007
8	0.452	0.537	0.451	0.457	0.500	0.519	0.225 ± 0.006
9	0.424	0.448	0.473	0.472	0.446	0.540	0.226 ± 0.012
10	0.395	0.443	0.499	0.484	0.463	0.447	0.228 ± 0.002
11	0.427	0.412	0.503	0.543	0.529	0.476	0.240 ± 0.009
12	0.409	0.441	0.441	0.429	0.495	0.485	0.242 ± 0.009
13	0.410	0.498	0.449	0.344	0.383	0.459	0.244 ± 0.010
14	0.370	0.443	0.375	0.400	0.379	0.419	0.228 ± 0.004

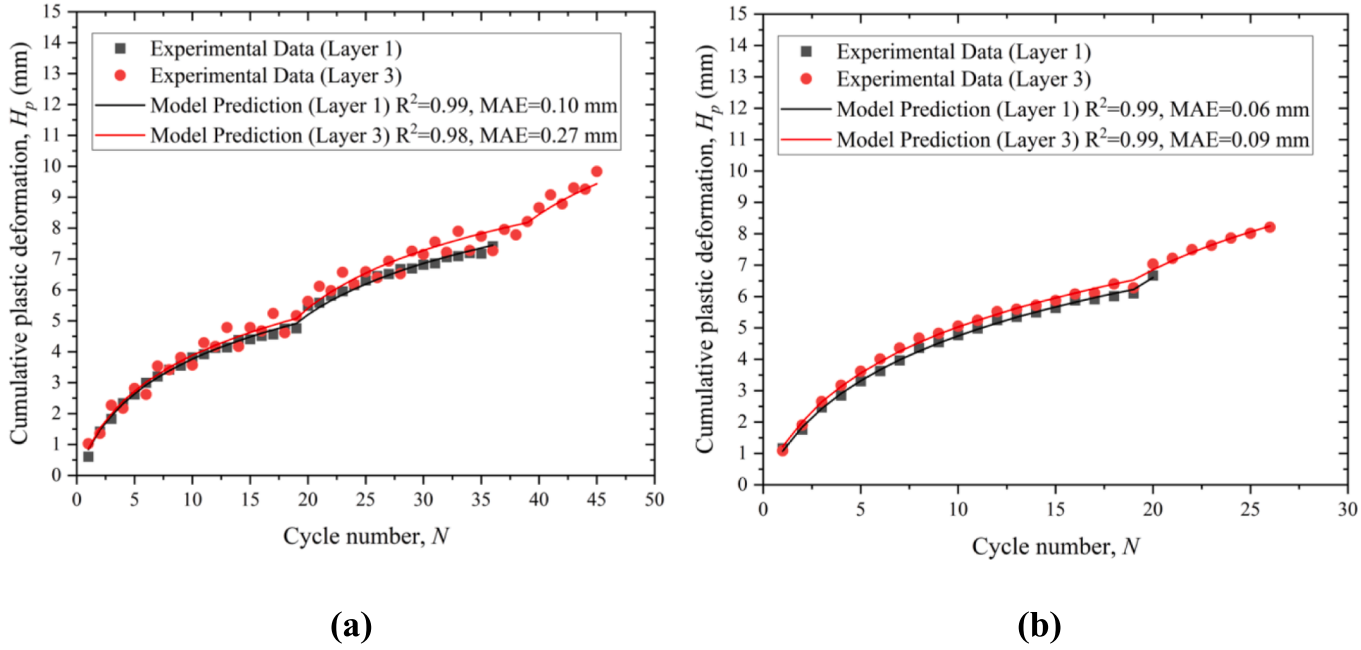

Fig. 8. Prediction ability of the developed model for two layers each for (a) sample 4 and (b) sample 13.

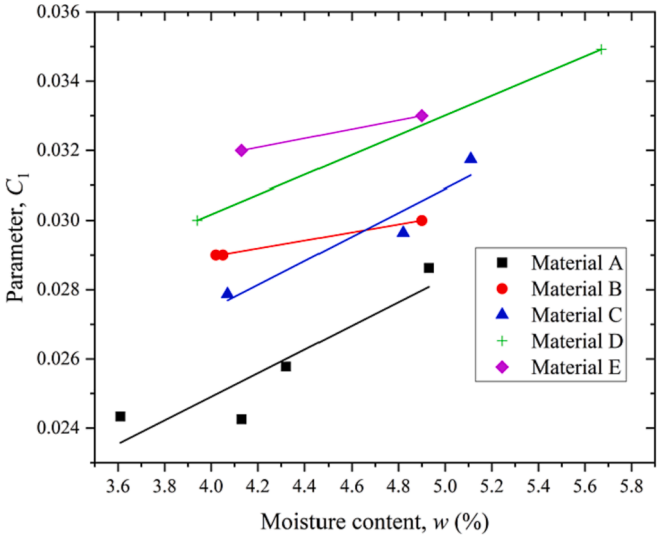

Fig. 9. Variation of model parameter C_1 with moisture content (w).

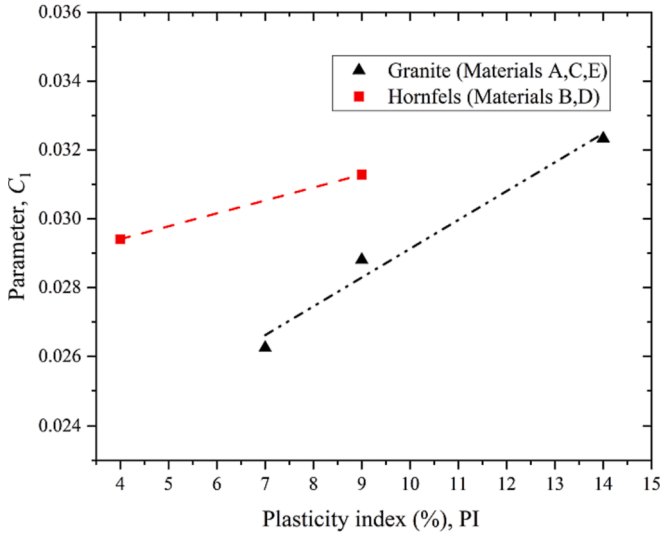

Fig. 10. Effect of plasticity on model parameter C_1 at moisture content 4.4%.

represents the number of values of Y.

Fig. 8 shows the model prediction ability for two examples (Sample 4 and Sample 13) for two layers (layer 1 and layer 3). Both figures illustrate that the model was an excellent predictor for the observed data even when the load increment was required (cycle number 20 and cycle number 40 for sample 4 and cycle 20 for sample 13). Only four examples are shown for clarity, but the proposed model showed excellent prediction skill for the entire dataset with R^2 >0.98 and MAE of less than 0.3 mm.

Constitutive Parameter estimation

The two new constitutive parameters α and β were estimated as 15 mm and 0.25 respectively for all the materials, for the given compactor evaluated using the least square method. Parameters C_1 and m were also evaluated using the least square method. The parameter C_1 was found to be the same for a given material, independent of the initial density of the sample. However, C_1 was a function of sample moisture content (Fig. 9) which was also reported in the authors' previous work for constant stress 1D compaction tests [8].

According to Equation (15), the value of C_1 is directly proportional to the strain accumulated for a given stress. Fig. 9 indicates that the value increases with an increase in moisture content. This is in line with the Proctor compaction theory, stating that the compaction (i.e. height reduction) is easier when the moisture is higher (note that all the compaction moisture content were lower than OMC obtained from the modified Proctor test) [29,30]. As all the tests were performed dry of optimum and, therefore, conclusions regarding wet of optimum are not made in this article. The authors however believe that conclusions made in previous studies (e.g., ([29,31])) that the compaction is difficult with an increase in the water content when compacted wetter than the optimum is valid for this study as well.

Fig. 9 also highlights that the for the materials used, higher the plasticity index, the better the compaction for the materials used as

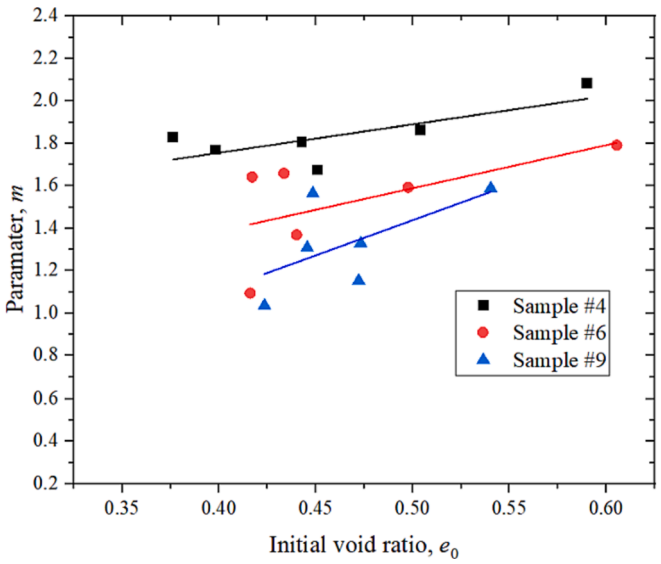

Fig. 11. Variation of model parameter m with initial void ratio (e_0).

reflected by the corresponding values of C_1. For a better illustration, Fig. 10 is plotted which shows the variation of model parameter C_1 for different materials at one moisture content (4.4%). The variation confirms that as the plasticity index increase value of model parameter C_1 increases.

The model parameter m was found to be linearly dependent on initial density (e_0), as observed in Fig. 11 for the three example samples. The values of m on the entire dataset are in Table 5. The linear dependency between m and e_0 was also reported in the authors' previous work [8], where samples tested under 1D compaction had the model parameter strongly related to the initial density. The relationship between parameter m and e_0 was also evaluated when m was considered independent of e_0 as shown in the last column of Table 5. When m was considered independent of e_0 the prediction error of the model increased, but this needs to be balanced with the need for parameter reduction, especially for real-time applications of the developed model.

Evolution of contact width, stress and stiffness parameters during compaction

In order to demonstrate the parameter evolution with cyclic compaction, contact width (B), contact stress (σ), modulus (E_1), and stiffness (K) due to the dynamic loading, interactions between the roller and geomaterial were calculated and plotted for sample 4, layers 1 and 5 below. These particular sample and layers were chosen to contrast the material properties as they needed 36 and 94 cycles to reach the final void ratio (e_{final}). Only two stages were applied for layer 1 while all stages of loading were applied for the layer 5, facilitating a better illustration of the parameter evolution. The two independent parameters e_N and the cycle number N were chosen because it is easier to track or measure them in the lab and field. Fig. 12 shows the geomaterial property variation with e_N in the multi-stage loading. The x-axis in all subfigures is plotted in the reverse order as it decreases during compaction for easy visualisation. The parameters σ, E_1, and K increased during compaction as the material gets stiffer, therefore, having an inverse relationship with the e_N, which reduces with compaction.

Conversely, the contact width (B) reduced during compaction giving rise to an increase in the contact stress (σ) and therefore had a positive relationship with e_N. It can be observed that on each occasion the applied load was increased (as the loading stage is changed), the parameters E_1, B, and σ increased and K reduced.

Fig. 13 shows the variation of parameters with the numbers of cycles of compaction. Since e_N and N are inversely related, the variations of all parameters with e_N and N are opposite.

Due to the difference in the loading history, the modulus at the final void ratio is different and is higher for the sample that had a higher initial void ratio. The observation could be attributed to the difference in the load (10 kN for layer 1 and 30 kN for layer 5) at the final loading stage. At the final compaction cycle, the contact width was around 7 mm for layer 5, which was lower when compared to layer 1 where the contact width was 8.2 mm. The other material properties (modulus, stress and stiffness) were higher for layer 5 compared to layer 1. This could be because the final load applied was higher for layer 5. The other possible reason could be the complex non-linear mulit-dimensional interaction of contact mechanics between the compactor and the material, which needs further investigation.

Table 6 presents simplified relationships for all the parameters including when the applied load (F) is constant with e_N and N. C_0 to C_{10} in the table are model parameters. For example, all the parameters can be expressed as an exponential function of e_N. Conversely, variation of all parameters can be expressed as a power function of N except for K, which can be expressed as a linear function of N. These equations can be used directly to calibrate the model parameters if a similar test setup involving a roller is used, either in the field or in the lab. And also can be used for finite element modelling etc., and their variation/evolution with e_N and N can be used instead of considering them constant during compaction.

Total energy imparted to the sample to achieve the target density

The cumulative energy required to achieve the target density is an important parameter for the optimal construction of pavement layers. It dictates the number of passes required to achieve the desired

Table 5
Value of parameter m obtained for all 14 samples having six layers.

Sample ID	Layer 1	Layer 2	Layer 3	Layer 4	Layer 5	Layer 6	Void ratio independent*
1	2.09	1.96	2.07	1.91	2.02	1.78	1.92
2	1.72	1.69	1.80	1.66	1.76	1.56	1.67
3	0.93	1.82	1.65	1.77	1.58	1.50	1.65
4	1.83	1.77	1.81	1.86	2.08	1.67	1.98
5	0.97	1.29	2.07	1.35	1.39	1.30	1.34
6	1.09	1.37	1.66	1.59	1.64	1.79	1.70
7	0.44	2.23	1.94	2.25	1.86	1.39	1.94
8	1.75	1.60	1.40	1.37	1.59	1.50	1.55
9	1.04	1.56	1.33	1.15	1.31	1.59	1.37
10	1.26	1.61	1.41	1.24	1.95	2.22	1.46
11	0.82	0.97	1.18	1.24	1.01	0.71	1.10
12	1.25	1.80	1.56	1.46	1.98	1.41	1.63
13	1.85	1.74	1.81	2.12	1.81	2.35	1.81
14	0.62	2.06	2.05	1.63	1.18	1.74	1.90

* Considering the entire dataset for a sample.

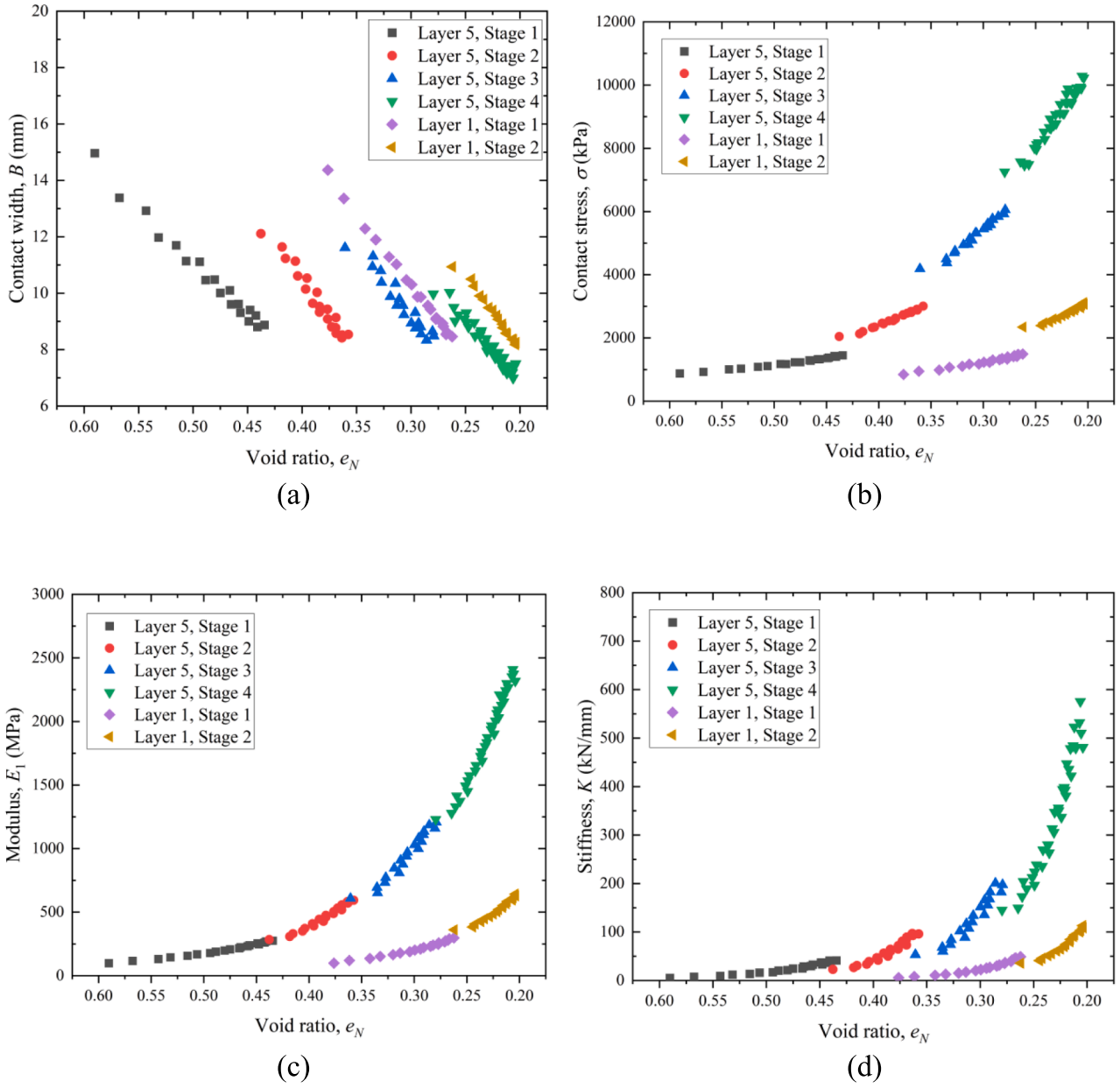

Fig. 12. Variation of parameters: (a) B, (b) σ, (c) E_1, (d) K with e_N during compaction.

specifications of the geomaterials. The optimal use of energy is also important for sustainable construction where energy utilization is optimised. In addition, compacting the material more than required can cause over-compaction, allowing the material to heave, with multiple shear planes and chaotic motions of the roller leading to breakdown and wear and tear of the rollers [32,33]. Over-compaction can also lead to excessive plastic deformation or rutting during the traffic loading in its service life [34–36].

The total energy applied per unit volume (ξ_{app}) to reach the final density or void ratio was calculated using the following equation as:

$$\xi_{app} = \frac{\sum_0^N F \times \Delta H_p}{H_0 \times B \times L} \tag{23}$$

The energy applied, ξ_{app}, to reach the target density (MDD for this study) was compared to the energy applied in the standard and modified Proctor tests. It was found that all samples needed less energy than the modified Proctor (2703 kJ/m^3 [36]). This was because the material was provided energy during manual tamping and spreading and therefore did not start from its loosest state. The manual tamping and spreading may to some extent replicate the paver spreading in the field; therefore, careful consideration of the number of delivered passes by the compactor should be considered. Fig. 14 illustrates the variation of ξ_{app} with e_0 for six samples (three samples for each of material B and material C). Two observations can be made; first, ξ_{app} is directly proportional to e_0; second, ξ_{app} is lower for higher moisture contents (increasing order of moisture content is sample 8, sample 9 and sample 10) at the same e_0, confirming the observation made in Fig. 9. The graph cannot be directly used for field compaction control using bigger rollers as the energy transfer mechanism, and energy losses are different in the two settings. To use the developed graph for field compaction control, a similar graph should be developed in the field for a particular compaction machine by measuring the thickness change using external devices such as a total station scanner and laser scanners.

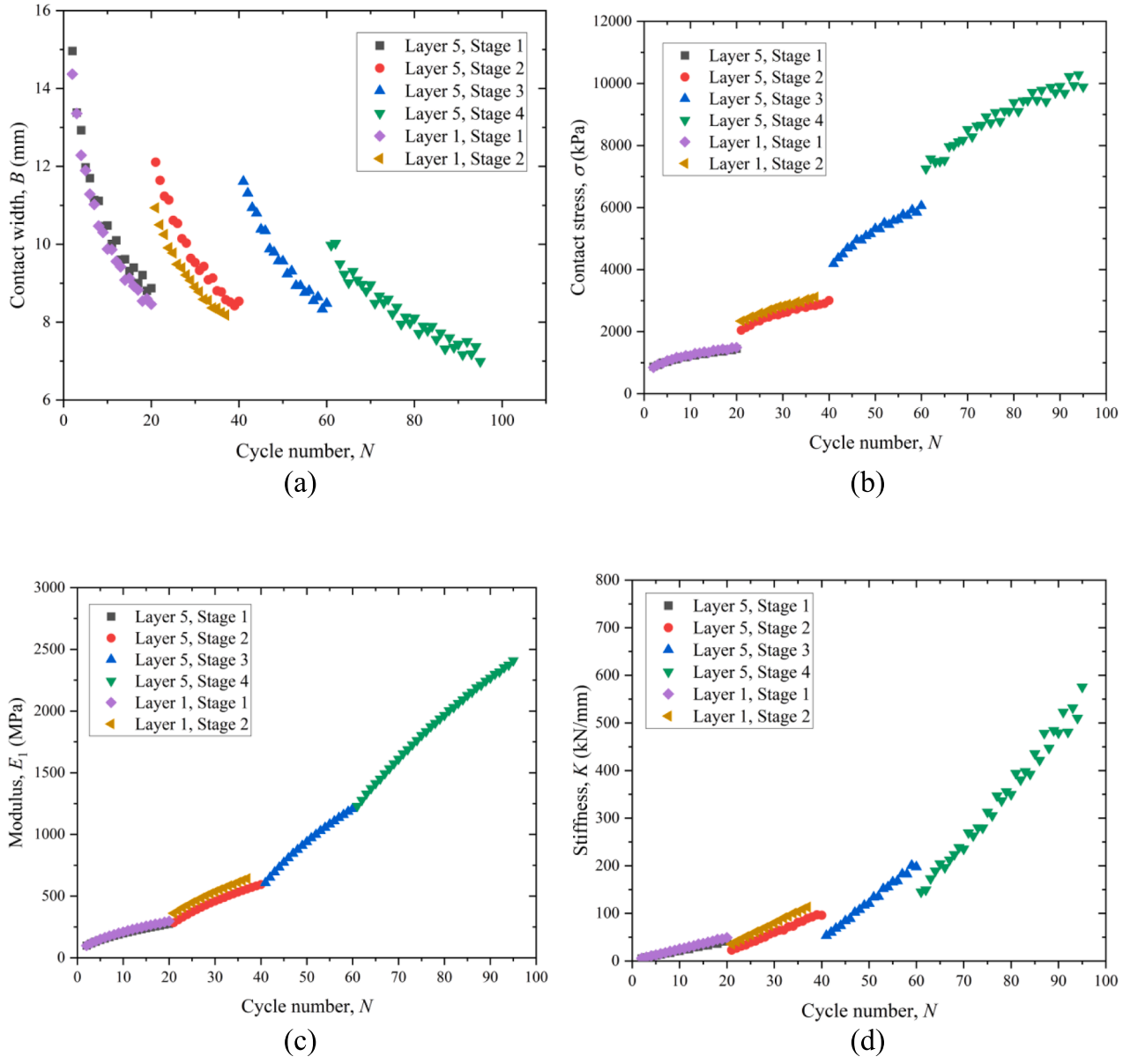

Fig. 13. Variation of parameters: (a) B, (b) σ, (c) E_1, (d) K with N during compaction.

Conclusions and implications of this study

Construction of any civil engineering structure requires earthwork activities, including embankment construction for dams and bridges. The geomaterials used are compacted using rollers to attain the properties required. To understand and optimise the compaction process, it is very important to understand the compaction process through modelling, and small-scale experiments in the lab, as repeating field-scale experiments requires a big investment. This study addressed the following major issues related to understanding the compaction process by testing UGMs in a simulated wheel tracking apparatus at different initial conditions (plasticity, moisture content (w) and initial void ratio (e_0)). They are as follows:

(a) Roller compaction modelling has been a challenge throughout. One reason is that the stress acting on the material properties are not constant during compaction. As the material gets stiffer during compaction, the contact area or width (B) between the drum and the geomaterial gradually reduces. Generally, the applied load (F) during compaction is constant; and the contact stress (σ) increases due to reduction of B. This is entirely different from tests usually carried out in a laboratory, where the stress is kept constant. Hence, the model developed from the constant stress test cannot be used to model the variable stress compaction process. This study extended a constant stress model to a constant load model using the geometrical relationship between B and incremental plastic deformation (ΔH_p). The excellent predictability of the simplified model shows that the complex compaction can be reasonably approximated using a simple 1D equation. The proposed model eliminates the requirement of a complex model, which hinders a real-time application as the computational time is high.

(b) Equations are presented where the dynamic parameters vary with the void ratio and the number of cycles. Simplified equations are also presented, which can be used by Finite element research instead of considering the stress or contact width as a constant.

(c) The effect of moisture content and plasticity was highlighted in various parts of this article, showing that moisture aids in

Table 6
Simplified equations for all the parameters for special case.

Parameter	Constant Load	Simplified equation with cycle No.	Simplified equation with void ratio
Contact width (B)	$B = \alpha(H_0C_1)^{\frac{\beta}{1+\beta m}}\left(1+\frac{1}{1+\beta m}\left(\frac{4F}{\pi L\alpha}\right)^m N\right)^{-\beta}$	$B = C_2{C_0}^{C_3}(1+C_4F^mN)^{-C_{10}}$	$B = C_2{C_0}^{C_3}exp(C_5\times(C_6-e_N))$
Contact Stress (σ)	$\sigma = (H_0C_1)^{\frac{-\beta}{1+\beta m}}\left(1+\frac{1}{1+\beta m}\left(\frac{4F}{\pi L\alpha}\right)^m N\right)^{\beta}$	$\sigma = {C_0}^{-C_3}(1+C_4F^mN)^{C_{10}}$	$\sigma = {C_0}^{-C_3}exp(-C_5\times(C_6-e_N))$
Modulus (E_1)	$E_1 = \frac{(H_0C_1)^{\frac{-2\beta}{1+\beta m}}\left(1+\frac{1}{1+\beta m}\left(\frac{4F}{\pi L\alpha}\right)^m N\right)^{2\beta}\times\left(\frac{\pi LR}{F}\right)E_2(1-\nu_1^2)}{E_2-(H_0C_1)^{\frac{-2\beta}{1+\beta m}}\left(1+\frac{1}{1+\beta m}\left(\frac{4F}{\pi L\alpha}\right)^m N\right)^{2\beta}\times\left(\frac{\pi LR}{F}\right)E_2(1-\nu_2^2)}$	$E_1 = \frac{C_8{C_0}^{-2C_3}(1+C_4F^mN)^{2C_{10}}}{FE_2-C_7{C_0}^{-2C_3}(1+C_4F^mN)^{2C_{10}}}$	$E_1 = \frac{C_8{C_0}^{-2C_3}exp(-2C_5\times(C_6-e_N))}{FE_2-C_7{C_0}^{-2C_3}exp(-2C_5\times(C_6-e_N))}$
Stiffness (K)	$K = (H_0C_1)^{\frac{-1}{1+\beta m}}\left(1+\frac{1}{1+\beta m}\left(\frac{4F}{\pi L\alpha}\right)^m N\right)$	$K = {C_0}^{C_9}(1+C_4F^mN)$	$K = {C_0}^{C_9}exp(-C_5\times(C_6-e_N))$

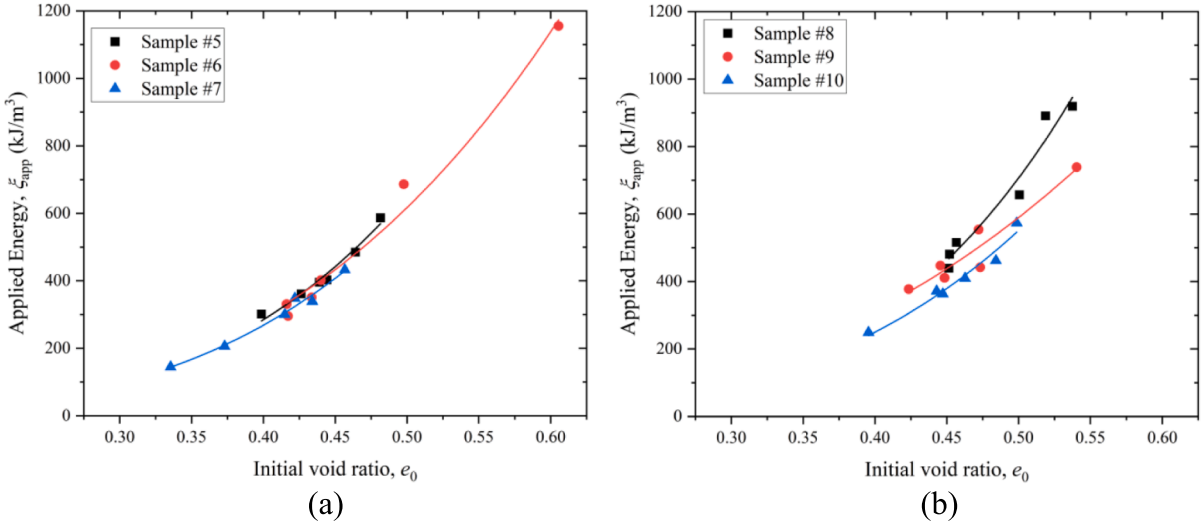

Fig. 14. Variation of total energy applied with e_N for: (a) material B, (b) material C.

compaction. This is in line with the Proctor compaction theory, as the moisture content used was less than optimal. Model parameter C_1 was higher for sample with higher moisture content and higher plasticity of fines.

(d) This study also highlights the effect of the initial void ratio on the parameters of the geomaterial during compaction. The different initial void ratios in the field can arise because of different spreading or paving techniques. The study of model parameters and their dependence on the initial void ratio is highlighted. The initial void ratio dependency is also important as it allows to study of the energy required to achieve a certain degree of compaction. This would ensure the sustainable use of compaction energy.

(e) Although the model was developed for static load using a drum compactor, the authors hypothesize that the concepts developed can be extended for vibratory drum compaction possibly by scaling the static load with the dynamic load applied by vibratory rollers. The information about vibratory compactors' eccentric mass is known, allowing the vibratory load estimation. The load term in the original model's equation representing the static load can be replaced with the combined dynamic load (static and vibratory load).

Funding.

This study was supported by the Australian Research Council (ARC) Industrial Transformation Research Hub (ITRH) Scheme (Grant No IH180100010). This project was also funded by Austroads through project TT1611 and TT1819.

Availability of data and material: Not applicable.

Code availability: Not applicable.

CRediT authorship contribution statement

Amir Tophel: Conceptualization, Methodology, Software, Formal analysis, Writing – original draft, Visualization. **Jeffrey P. Walker:** Resources, Writing – review & editing, Supervision, Project administration. **Troyee Tanu Dutta:** Writing – review & editing, Visualization, Supervision. **Didier Bodin:** Methodology, Investigation, Resources, Data curation, Writing – review & editing, Supervision, Project administration. **Jayantha Kodikara:** Conceptualization, Methodology, Resources, Writing – review & editing, Supervision, Project administration, Funding acquisition.

Declaration of Competing Interest

The authors declare that they have no known competing financial interests or personal relationships that could have appeared to influence the work reported in this paper.

Data availability

Data will be made available on request.

Acknowledgments

The first author received a Monash University Graduate Scholarship (MGS) to undertake this research project. This research work was also part of a research project (Project No IH18.03.3) sponsored by the SPARC Hub (https://sparchub.org.au) at the Department of Civil Engineering, Monash University, funded by the Australian Research Council (ARC) Industrial Transformation Research Hub (ITRH) Scheme (Project ID: IH180100010). The authors would like to acknowledge the Australian Road Research Board (ARRB) for providing the experimental data, and technical as well as in-kind support. The authors would also like to acknowledge Austroads for funding project TT1611 and TT1819. The authors gratefully acknowledge the financial and in-kind support of Monash University, SPARC Hub, CIMIC, and EIC activities.

References

[1] Chong SH, Santamarina JC. Sands subjected to repetitive vertical loading under zero lateral strain: accumulation models, terminal densities, and settlement. Can Geotech J 2016;53:2039–46. https://doi.org/10.1139/cgj-2016-0032.
[2] Park J, Santamarina JC. Sand response to a large number of loading cycles under zero-lateral-strain conditions: evolution of void ratio and small-strain stiffness. Geotechnique 2019;69:501–13. https://doi.org/10.1680/jgeot.17.P.124.
[3] Pasten C, Shin H, Santamarina JC. Long-term foundation response to repetitive loading. J Geotech Geoenviron Eng 2014;140:1–11. https://doi.org/10.1061/(ASCE)GT.1943-5606.0001052.
[4] Wichtmann T. Explicit accumulation model for non-cohesive soils under cyclic loading. Inst für Grundbau und Bodenmechanik Phd:274; 2005. PhD Thesis.
[5] Modoni G, Koseki J, Anh Dan LQ. Cyclic stress-strain response of compacted gravel. Geotechnique 2011;61:473–85. https://doi.org/10.1680/geot.7.00150.
[6] Pestana JM, Whittle AJ, Salvati LA. Evaluation of a constitutive model for clays and sands: Part I - sand behaviour. Int J Numer Anal Methods Geomech 2002;26:1097–121. https://doi.org/10.1002/nag.237.
[7] Sawicki A, Swidzinski W. Cyclic compaction of soils, grains and powders. Powder Technol 1995;85:97–104. https://doi.org/10.1016/0032-5910(95)03013-Y.
[8] Tophel A, Walker JP, Dutta TT, Kodikara J. Theory-guided machine learning to predict density evolution of sand dynamically compacted under Ko condition. Acta Geotech 2022. https://doi.org/10.1007/s11440-021-01431-2.
[9] Hager M, Pistrol J, Kopf F, Adam D. Verdichtung mit Vibrationswalzen. Bauingenieur: Semi-analytische Modellierung des Interaktionssystems Bandage-Boden mit Berücksichtigung der veränderlichen Bandagenaufstandsbreite; 2021. p. 96.
[10] G, Kargl Modellversuche zur Ermittlung des Last-Deformationsverhaltens geschichteter Modellböden unter ebenen und zylindrisch gekrümmten Belastungsflächen und vergleichende Computerberechnungen. TU Wien 1995.
[11] Ghorbani J, Nazem M, Kodikara J, Wriggers P. Finite element solution for static and dynamic interactions of cylindrical rigid objects and unsaturated granular soils. Comput Methods Appl Mech Eng 2021;384:113974. https://doi.org/10.1016/j.cma.2021.113974.
[12] Hertz H. Über die Berührung fester elasticscher Körper (On the contact of elastic body). Leipzig: Gesammelte Werke; 1895.
[13] B, Caicedo Geotechnics of Roads: Fundamentals. CRC Press, Taylor & Francis Group 2019.
[14] Rinehart RV, Mooney MA. Measurement of roller compactor induced triaxial soil stresses and strains. Geotech Test J 2009;32:347–57. https://doi.org/10.1520/gtj101889.
[15] Kenneally B, Musimbi OM, Wang J, Mooney MA. Finite element analysis of vibratory roller response on layered soil systems. Comput Geotech 2015;67:73–82. https://doi.org/10.1016/j.compgeo.2015.02.015.
[16] Tatsuoka F, Hashimoto T, Tateyama K. Soil stiffness as a function of dry density and the degree of saturation for compaction control. Soils Found 2021;61:989–1002. https://doi.org/10.1016/j.sandf.2021.06.007.
[17] Tophel A, Kodikara J, Walker JP. Systems and methods for measuring/estimating geomaterial layer properties due to compaction. Patent Cooperation Treaty (PCT) 2021. AU2021/051505.
[18] Tophel A, Walker J, Lu Y, Kodikara J. Proximal sensing of density during soil compaction by instrumented roller. Aust Geomech J 2022;57:161–9. https://doi.org/10.56295/AGJ5739.
[19] A, Tophel, JP, Walker, TT, Dutta, J, Kodikara Using a Novel Instrumented Roller to Estimate Soil Dry Density During Compaction. In: Gomes Correia A, Azenha M, Cruz PJS, et al (eds) Trends on Construction in the Digital Era. ISIC 2022. Lecture Notes in Civil Engineering, vol 306. Springer, Cham 2023, pp 538–546.
[20] Bodin D. Improved laboratory characterisation of the deformation properties of granular materials. Austroads Publ AP-T324-17 2017.
[21] D, Bodin, M, Moffatt, G, Jameson Development of a Wheel-tracking Test for Rut Resistance Characterisation of Unbound Granular Materials. Austroads Publ AP-T240-13 2013.
[22] VicRoads (2016) Crushed Rock for Pavement Base and Subbase. http://webapps.vicroads.vic.gov.au/VRNE/csdspeci.nsf/webscdocs/A633FC705037997BCA257FEF0003DBF6?OpenDocument. Accessed 2 Jul 2022.
[23] Standards Australia (2009) Soil classification tests- Determination of the particle size distribution of a soil—Standard method of analysis by sieving. AS 1289361.
[24] Standards Australia (2009) Soil classification tests - Determination of the plastic limit of a soil - Standard method. AS 1289321.
[25] Standards Australia (2009) Soil classification tests - Determination of the liquid limit of a soil - One point Casagrande method (subsidiary method). AS 1289312.
[26] Standards Australia (2009) Soil classification tests - Calculation of the plasticity index of a soil. AS 1289331.
[27] Standards Australia (2002) Soil classification tests— Determination of the soil particle density of combined soil fractions—Vacuum pycnometer method. AS 1289352.
[28] Australia S. Soil compaction and density tests — Determination of the dry density / moisture content relation of a soil using modified compactive effort. AS 2003;1289521:1–13.
[29] Kodikara J. New framework for volumetric constitutive behaviour of compacted unsaturated soils. Can Geotech J 2012;49:1227–43. https://doi.org/10.1139/t2012-084.
[30] Kodikara J, Islam T, Sounthararajah A. Review of soil compaction: History and recent developments. Transp Geotech 2018;17:24–34. https://doi.org/10.1016/j.trgeo.2018.09.006.
[31] Tatsuoka F, Gomes Correia A. Importance of controlling the degree of saturation in soil compaction linked to soil structure design. Transp Geotech 2018;17:3–23. https://doi.org/10.1016/j.trgeo.2018.06.004.
[32] Liu D, Wang Y, Chen J, Zhang Y. Intelligent compaction practice and development: a bibliometric analysis. Eng Constr Archit Manag 2019;27:1213–32. https://doi.org/10.1108/ECAM-05-2019-0252.
[33] Anderegg R, Kaufmann K. Intelligent compaction with vibratory rollers: feedback control systems in automatic compaction and compaction control. Transp Res Rec J Transp Res Board 2004;1868:124–34. https://doi.org/10.3141/1868-13.
[34] Monismith CL, Ogawa N, Freeme CR. Permanent deformation characteristics of subgrade soils due to repeated loading. Transp Res Rec 1975;537.
[35] Brown SF, Hyde AFL. Significance of cyclic confining stress in repeated-load triaxial testing of granular material. Transp Res Rec 1975;537. https://doi.org/10.1016/0148-9062(76)90013-9.
[36] Lekarp F, Dawson A. Modelling permanent deformation behaviour of unbound granular materials. Constr Build Mater 1998. https://doi.org/10.1016/S0950-0618(97)00078-0.